Algorithm to Derive Narrow Band to Broad Band Albedo for Snow Using AWiFS and MODIS Imagery of Western Himalaya - Validation

Varunendra Dutta Mishra[1], Hemendra Singh Gusain[2], Manoj Kumar Arora[3]

[1, 2]Snow and Avalanche Study Establishment, Research & Development Centre, Chandigarh, India

[3]Department of Civil Engineering, Indian Institute of Technology, Roorkee, India

[1]vd_mishra@rediffmail.com; [2]gusain_hs@yahoo.co.in; [3]manoj.arora@gmail.com

***Abstract*-In this paper, algorithms to estimate narrowband to broadband albedo (NBBA) of snow using Advanced Wide Field Sensor (AWiFS) and Moderate Resolution Imaging Spectro-radiometer (MODIS) sensor images have been developed for Indian western Himalayan region. The in-situ measurements of spectral reflectance and transmitted spectral solar irradiance on snow surface by spectroradiometer have been used to calibrate and validate the algorithms developed. The AWiFS and MODIS derived snow broadband albedo via the developed algorithms have been validated with in-situ observations at three field locations. An RMSE better than 0.03 and an R^2 value of 0.94 and 0.88 between modeled and observed albedo values have been obtained for AWiFS and MODIS respectively. The algorithm developed for MODIS images has also been compared with an existing global albedo model for MODIS, and the results from the proposed model have been found to be in agreement with the published model.**

Keywords- Spectral; Broadband; Albedo; AwiFS; MODIS

I. INTRODUCTION

Broadband snow albedo in solar wavelength region (0.3 μm - 3.0 μm) has been an important parameter for various climatic studies. It is a key input to local or basin scale snowmelt runoff models and is also a significant parameter to understand and characterize the energy fluxes at the earth surface [1]. It also happens to be a pointer to understand many physical aspects of the snow surface, such as snow depth, grain size and water content [2]. Thus, the spatial variability of snow surface albedo is of immense importance in many applications such as ecosystem dynamics, hydrology, geomorphology and microclimate of high relief environments [3]. Variability in snow albedo exerts significant impact on snow cover properties during the course of accumulation and ablation.

Large stretch of mountainous regions in Himalaya is covered by permanent snow cover, which increases manifolds during winter season. Seasonal snow cover generally builds up and ablates from November to June in different ranges of lower and middle Himalaya [4]. Recent analyses of long term observations of snow precipitation show a declining trend of snowfall in Beas basin of Himalayan region [5]. The snow cover in mountainous region results in a cooler climate there by affecting the local energy balance through reduced absorption of the solar radiation. The study of snowmelt of the seasonal snow cover therefore requires an understanding of spatial and temporal variability of albedo in the Himalayan region.

Satellite remote sensing offers a means to quantitatively estimate the surface reflectance in discrete spectral bands in large spatial area of inaccessible Himalayan terrain. However, this spectral reflectance may not be directly used for energy balance estimation as it requires a short wave integrated albedo in the reflective solar wavelength region. Therefore, an appropriate methodology to estimate broadband integrated albedo over a snow-covered area from spectral reflectance of snow in discrete satellite bands is required. The narrowband reflectance from medium (e.g. IRS AWiFS) and moderate (e.g. Terra MODIS) spatial resolution satellite data may have the potential to provide an estimation of integrated snow albedo using the NBBA algorithms at frequent time intervals due to their high temporal resolution.

Reference [6] has reported an extensive work on conversion of narrowband to broadband albedo (NBBA) for a number of satellite sensors including Terra Advanced Space borne Thermal Emission and Reflection Radiometer (ASTER), NOAA Advanced Very High Resolution Radiometer (AVHRR), Geostationary Operational Environmental Satellite (GOES Imager), LANDSAT 7 Enhanced Thematic Mapper Plus (ETM^+), Terra Multiangle Imaging Spectroradiometer (MISR), Polarization and Directionality of Earth's Reflectances (POLDER), SPOT VEGETATION and Terra MODIS. The listed algorithms have been testified under different atmospheric conditions and solar geometry through MODTRAN, discrete-ordinate radiative transfer (DISORT) and other atmospheric correction models. Previous studies have established accurate estimation of broadband albedo from the Advanced Very High Resolution Radiometer (AVHRR) satellite data in polar region [7, 8]. Due to improved spectral/spatial characteristics and measurement precision of MODIS images as compared to AVHRR, it is anticipated that accuracy of surface albedo estimation may further increase. Reference [9] has applied MODIS Level 1B data to derive the albedo over Greenland. The satellite-derived surface albedo has been found to be within about 6% of that measured at the stations. Reference [1] has developed a prototype snow albedo algorithm that also relies on MODIS atmospherically corrected surface reflectance. However, it accounts for reflectance anisotropy using DISORT model. Reference [10] has developed a direct retrieval algorithm that links top-of-atmosphere (TOA) narrowband albedo to land surface broadband albedo using a feed-forward neural network. The algorithm, although, has been designed for

estimating albedo over any land cover types but appears to be particularly well designed for non-vegetated land cover. Moreover, it does not take into account atmospheric correction and other processes. Reference [11] has given a series of formulae for conversion of NBBA based on extensive radiative transfer simulations for data from different satellite sensors. One of the algorithms given in [10] has later been revised and applied to MODIS data for global albedo estimation [12].

The AWiFS data have very different spatial and spectral resolutions as compared to data from other remote sensing sensors. Therefore, the broadband albedo model developed for other sensors may not be directly applicable to AWiFS data. In the present study, an algorithm for narrowband to broadband albedo of snow using AWiFS data has been developed. The same methodology has also been extended to develop the algorithm for NBBA of snow using MODIS data. The efficacy of the algorithm for NBBA has been tested with the published algorithm for estimation of global albedo of snow using MODIS. The proposed algorithm uses narrow band reflectance of snow in visible (VIS), near-infrared (NIR) and short wave infrared (SWIR) bands.

II. STUDY AREA DESCRIPTION

The first study area lies between latitude 32˚ 12'N to 32˚ 60'N and longitude 77˚E to 77˚30'E and has been marked as ABCD on a map of India (Fig. 1a).

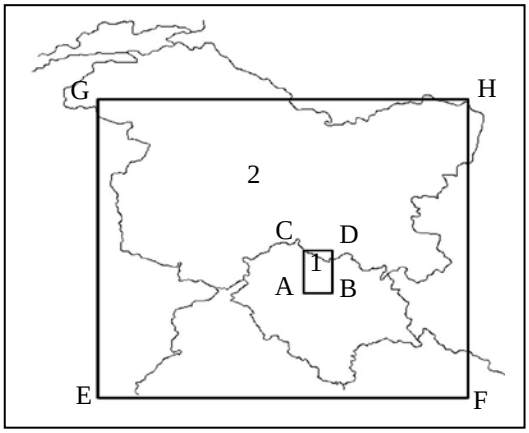

Fig. 1a) First study area marked with rectangle (ABCD) on India map

The AWiFS image corresponding to this area is shown in Fig. 1b.

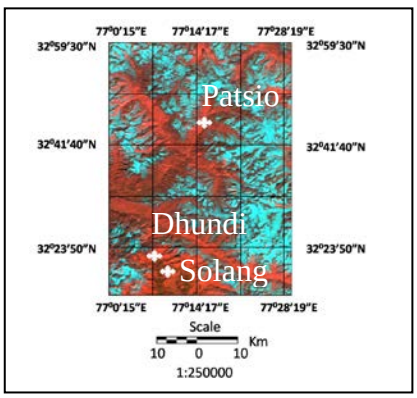

Fig. 1b) First study area ABCD and three field locations on AWiFS image for in-situ measurements of albedo for validation with satellite

The study area includes three scientific field observatories, namely, Solang (latitude 32˚19'27" N, longitude 77˚09'27"E), Dhundi (latitude 32˚21'22"N, longitude 77˚07'42"E) and Patsio (latitude 32˚45'11"N, longitude 77˚15'42"E) of Snow and Avalanche Study Establishment (SASE) in India. These observatories are responsible for collection of a variety of in-situ data including albedo measurement of snow at different time intervals. Solang and Dhundi observatories are located in the Beas basin in the Pir-Panjal Mountain range at altitudes of 2480 m a.s.l and 3050 m a.s.l respectively. The area is surrounded by forest and tree line which exists up to 3100 m a.s.l.. The Patsio observatory lies in the Greater Himalayan range at an altitude of 3880 m a.s.l and is devoid of forest. The two mountain ranges have different climatic and geomorphologic conditions. The monthly averaged minimum temperature during winter has been observed to be from -4.1^{o}C to 2.5^{o}C in Pir-Panjal range and from -6.4^{o}C to -15.4^{o}C in Greater Himalayan range [4]. Pir-Panjal range receives higher seasonal snowfall (with season average of 10-12 m) as compared to Greater Himalayan range (with season average of 5-7 m). The slope in the study area varies from 1 to 86 degree with a mean value of 28 degree. Most of the slopes in this study area are southern.

The second study area, marked as EFGH in Fig. 1a, lies between latitude 30˚0'0"N to latitude 36˚0'0"N and longitude 73˚0'0"E to 80˚0'0"E. The MODIS image corresponding to this area is shown in Fig. 2.

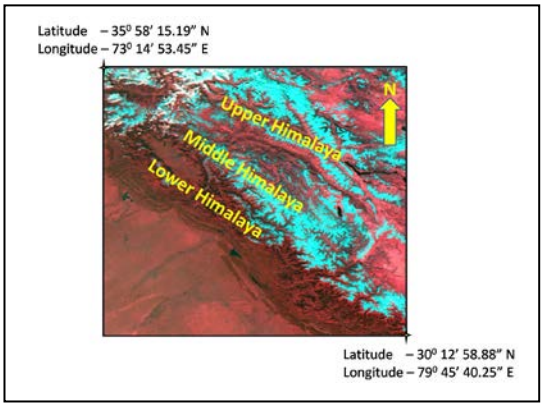

Fig. 2 Different Himalayan ranges corresponding to EFGH (Fig. 1a) on MODIS image used for proposed broadband albedo model comparison with reported global (Liang model) model

This area, having a larger areal extent than the first study area, has been used for validation of the proposed algorithm and its evaluation vis-a-vis published global albedo model for MODIS. This has been done to assess the efficacy of the proposed algorithm for a large snow covered area having varied topographic and meteorological conditions. The area mainly encompasses three different Himalayan zones, e.g., Lower Himalayan or Subtropical Zone, Middle Himalayan or Mid Latitudinal Zone and Upper Himalayan or High Latitudinal Zone, as described in detail in [13].

III. IN-SITU MEASUREMENTS OF SPECTRAL REFLECTANCE

Extensive in-situ measurements of spectral reflectance and transmitted solar irradiance on snow in the wavelength

range from 350 to 2500 nm have been recorded simultaneously at the time of satellite passes near Solang and Dhundi observatories. Field Spec Pro spectroradiometer (M/S Analytical Spectral devices, USA), shown in Fig. 3a has been used to collect measurements of snow at 25˚ field of view (FOV) under clear sky conditions on nearly flat surface. Simultaneously, solar transmitted spectral irradiances have also been measured using a full sky remote cosine receptor having a 180˚ FOV. These in-situ measurements have been used for NBBA model development and validation of the data acquired from AWiFS and MODIS at Solang and Dhundi sites. The results from NBBA model for AWiFS and MODIS data have also been validated at Patsio, where in-situ measurements of albedo have been collected using Albedometer at the time of satellite passes. Albedometer, mounted on an Automatic Weather Station (AWS), consists of two CMP3 pyranometers (Kipp and Zonen) with one looking up towards sky and another looking down towards snow surface (Fig. 3b).

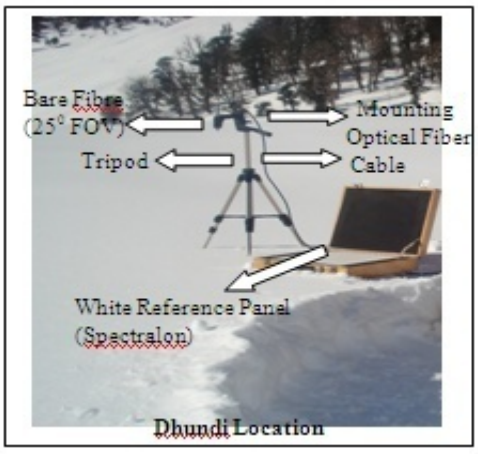

Fig. 3a) Optical Spectro-radiometer and its different components at snow covered Dhundi location

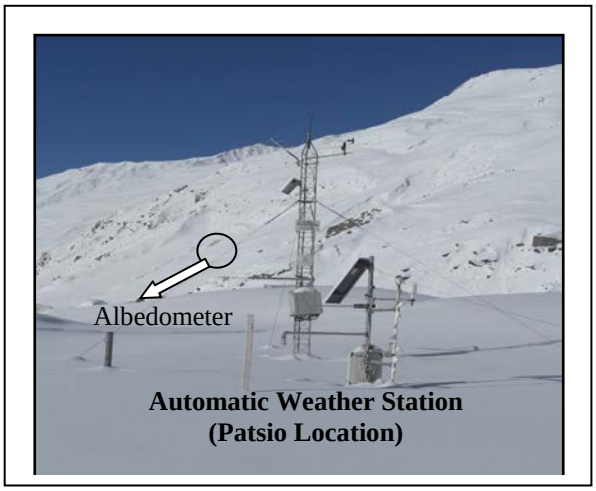

Fig. 3b) Albedometer (two pyranometers CMP3) for broadband albedo measurements mounted on Automatic Weather Station at Patsio location

IV. SATELLITE SENSOR DATA

Almost clear sky multi-spectral medium spatial resolution (56 m) and 10-bit radiometric resolution data obtained from AWiFS on-board RESOURCESAT-I and moderate resolution (250 m and 500 m) having radiometric resolution 12 bit obtained from MODIS on-board Terra have been used in this study. The salient characteristics of AWiFS and MODIS sensors have been given in the Table I and TableII respectively. Twelve AWiFS images and nine MODIS images (Table III) of different dates have been used for NBBA model development and its validation using in-situ observations.

TABLE I SALIENT SPECIFICATIONS OF AWIFS SENSOR

Spectral Bands	Spectral Wavelength (nm)	Maximum Radiance ($mW/cm^2/sr/\mu m$)	Solar Exoatmospheric Spectral Irradiance ($mW/cm^2/\mu m$)
B2	520-590	52.34	185.3281
B3	620-680	40.75	158.042
B4	770-860	28.425	108.357
B5	1550-1700	4.645	23.786

TABLE II SALIENT SPECIFICATIONS OF MODIS SENSOR

Spec-tral Bands	Spectral wave-length (nm)	Spatial Resolu-tion (m)	Radiance_ Scale ($mW/cm^2/sr/\mu m$)	Solar Exoatmosphe-ric Spectral Irradiance ($mW/cm^2/\mu m$)
B1	620-670	250	0.0026144	160.327
B2	841-876	250	0.0009926	98.70
B3	459-479	500	0.0027612	209.071
B4	545-565	500	0.0021087	186.4
B5	1230-1250	500	0.0005568	47.6
B6	1628-1652	500	0.0002572	23.8
B7	2105-2155	500	0.0000787	8.7

TABLE III DATES OF ACQUISITION OF AWIFS AND MODIS IMAGES USED

S.No.	AWiFS Images	MODIS Images
1	19 January 2005	26 December 2008
2	21 February 2005	31 December 2008
3	26 February 2005	20 January 2009
4	13 March 2005	28 January 2009
5	7 March 2007	30 January 2009
6	8 January 2009	26 February 2009
7	24 December 2008	16 March 2009
8	31 January 2009	13 April 2009
9	15 February 2009	17 April 2009
10	25 February 2009	
11	11 March 2009	
12	16March 2009	

V. TOPOGRAPHY OF STUDY AREA

A digital elevation model (DEM) of the study area ABCD (Fig. 1a) has been generated from on-screen digitization of contours on topographical map at 1:50000 scale at 40 m contour interval and is shown in the Fig. 4a. A non-linear interpolation function has been used for DEM generation. The DEM has been re-sampled from 6 m to 56 m to match the spatial resolution of AWiFS image. From this DEM, other topographic parameters, namely, slope (Fig.

4b), aspect (Fig. 4c) and local illumination image have been derived for terrain corrections using slope match method.

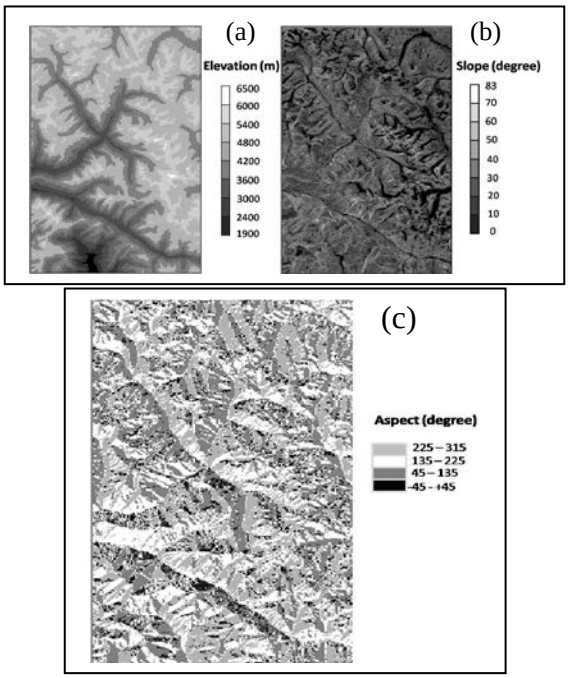

Fig. 4a) Digital elevation model; b) Slope and c) Aspect of study area ABCD at 6m spatial resolution

VI. METHODOLOGY

Snow covered surfaces are usually characterized by very high spectral reflectance in the visible wavelength region, which rapidly decreases in NIR and SWIR regions. Thus, reflectance in narrow bands in VIS and SWIR regions of AWiFS and MODIS sensors appear very dominant in characterizing snow surface conditions. Therefore, data from three bands of AWiFS (Bands 2, 4 and 5) and seven bands of MODIS (Band1-Band7) have been used to develop the algorithm for NBBA of snow. The flow chart of detailed methodology for NBBA is given in the Fig. 5.

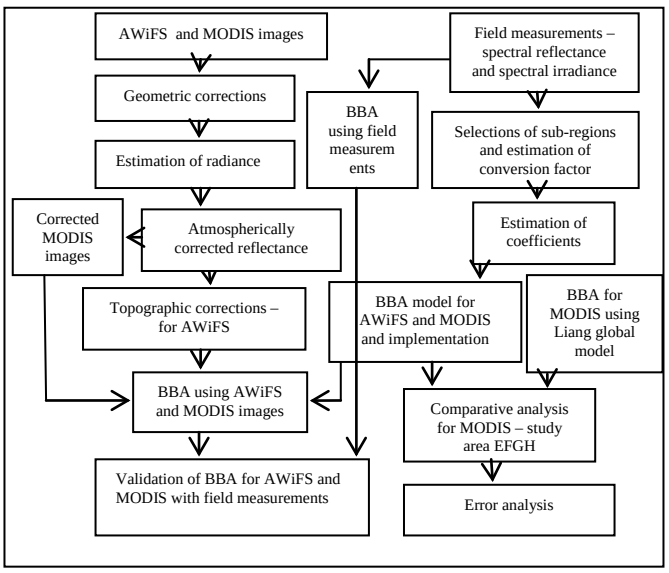

Fig. 5 Flow chart showing methodology for model development of broadband albedo and validation

First, image based atmospheric corrections for path radiance without considering topographic influences and Rayleigh scattering was performed for initial estimates of reflectance at each pixel of AWiFS and MODIS images [14, 15]. The AWiFS reflectance image was further refined by applying topographic correction using slope matching method, which is reported to be the most suitable method for Himalayan region [16]. The topographic correction on MODIS reflectance image has not been applied due to its moderate spatial resolution [17].

All the AWiFS and MODIS images have been geometrically and atmospherically corrected before the estimation of spectral reflectance at each pixel.

A. Geo-Referencing

Available geocoded IRS-LISS-III (Indian Remote Sensing, Linear Imaging Self Scanning) image was used as the master image for geo-referencing of AWiFS images. The MODIS images were then georeferenced to AWiFS images. The geo-referencing of images has been performed using second order polynomial transformation at root mean square error of less than a pixel estimated using 18-20 ground control points (GCPs).

B. Atmospheric Correction

First, the digital numbers of pixels in AWiFS images have been converted to at-sensor spectral radiance, $L_{sat\,\lambda}$ (mWcm^{-2}Sr^{-1}μm^{-1}) using the following relationship,

$$L_{sat\,\lambda}(AWiFS) = \frac{L_{max\,\lambda} - L_{min\,\lambda}}{DN_{max\,\lambda}} DN_{sat\,\lambda} + L_{min} \qquad (1)$$

where $DN_{max\,\lambda}$ and $DN_{sat\,\lambda}$ are maximum and at-satellite DN values respectively in different AWiFS spectral bands. $L_{max\,\lambda}$ and $L_{min\,\lambda}$ are the maximum and minimum values of spectral radiance in different bands, as obtained from sensors' header information. $L_{min\,\lambda}$ = 0 and $DN_{max\,\lambda}$= 1023.

At satellite spectral radiance, $L_{sat\,\lambda}$, for each pixel of MODIS images in different bands is calculated using the (2) :

$$L_{sat\,\lambda}\,(MODIS) = radiance\_scales_{\lambda} \times (DN - radiance\_offset_{\lambda}) \qquad (2)$$

where $radiance\_scales_{\lambda}$ and $radiance\_offset_{\lambda}$ (zero for all bands) are the scale and offset parameters, respectively as given in Table II.

The estimated values of at-satellite radiance at pixel were corrected using combination of dark object subtraction (DOS1 and DOS3) model [15] for atmospheric correction. It is a simple and efficient model for operational use in the absence of in-situ data of various atmospheric parameters such as aerosol, water vapor content, etc., at the time of image acquisition [18, 19]. The DOS1 model assumes no atmospheric transmittance loss and no diffused downward radiation at the surface [14]. DOS3 computes upwelling and downwelling radiation transmittances of the atmosphere to correct the image for path radiance resulting from the interaction of the electromagnetic radiation with molecules

and aerosols. It assumes Rayleigh scattering only. The optical thickness for Rayleigh scattering is obtained from the equation proposed by [20].

The values of transmittance using Rayleigh scattering are estimated for AWiFS and MODIS spectral bands and shown in the Table IV.

TABLE IV UPWELLING AND DOWNWELLING TRANSMISSIVITY DUE TO RAYLEIGH SCATTERING FOR AWIFS AND MODIS SPECTRAL BANDS

Transmiss-ivity	Ban-d1	Band 2	Band 3	Band 4	Band 5	Band 6	Band 7
AWiFS-"t_v"	-	0.935	0.965	0.986	0.999	-	-
AWiFS-"t_z"	-	0.911	0.952	0.980	0.998	-	-
MODIS-"t_v"	0.965	0.989	0.877	0.936	0.997	0.999	1.0
MODIS-"t_z"	0.941	0.981	0.801	0.895	0.996	0.999	1.0

The dark objects (e.g., shadow, deep clean water) are not absolutely dark [21] due to atmospheric scattering effects. Assuming 1% surface reflectance for the dark objects, the path radiance was estimated using the proposed model [14, 22, 23]. The spectral reflectance corrected for path radiance, under lambertian assumption, of each pixel in AWiFS and MODIS images is then computed using the following (3) [15, 24]:

$$R_\lambda = \frac{\pi(L_{sat\,\lambda} - L_p)\,d^2}{t_v(E_0 \cos\theta_z\, t_z + E_d)} \quad (3)$$

where t_v and t_z are the transmittances of the atmosphere in the viewing and illumination directions respectively, as determined from the equations proposed [15, 20]. E_0 is the exo-atmospheric spectral irradiances as given in Tables I and II. θ_z is the solar zenith angle at each pixel and estimated using [25] d is the earth-sun distance in astronomical units obtained from the approach given by [26]. E_d is the downwelling diffused radiation and has been assumed as zero according to [22]. L_p is the path radiance obtained from the approach given in [22]

C. Topographic Corrections Using Slope Match Method

A number of image based topographic correction methods (e.g., Cosine correction, C-correction, Minneart correction, statistical etc.) have been proposed [27, 28]. An extensive study on the feasibility of different topographic correction methods for the Himalayan region has been reported [16] and recommended slope matching method more appropriate for the region. Slope matching method is given in (4) and used for topographic correction in the present study:

$$R_\lambda^t = R_\lambda + (R_{\lambda max} - R_{\lambda min})\left(\frac{<cosi>s - cosi}{<cosi>s}\right)C_\lambda \quad (4)$$

where R_λ^t is topographically corrected spectral reflectance, R_λ is obtained from (3), $R_{\lambda max}$ and $R_{\lambda min}$ are the maximum and minimum spectral reflectance values as obtained from R_λ image, $<cosi>s$ is average value of illumination on south aspect, $cosi$ is illumination obtained from the equation proposed by [27]. C_λ is the normalization coefficient for different bands and is estimated using equation given by [29].

D. Narrow Band Reflectance (NBR) to Broadband Albedo (BBA) From AWiFS and MODIS

Reference [30] has proposed an approach to convert NBR to BBA from Advance Very High Resolution Radiometer (AVHRR) image acquired in two bands. The same approach has been adopted here to derive a new algorithm considering three spectral bands (Band 2, Band 4 and Band 5) of AWiFS image (Table I) and seven spectral bands (Band 1 – Band 7) of MODIS image (Table II).

The surface integrated albedo, a, in any wavelength interval, $\Delta\lambda$, defined as the ratio of the integrated reflected energy, $\sum E_{s\Delta\lambda}\,\rho_{\Delta\lambda}$, to the integrated downward irradiance, $\sum E_{s\Delta\lambda}$, at the solar zenith angle, θ_z and can be expressed as [12]:

$$a = \frac{\sum_{\Delta\lambda} E_{s\Delta\lambda}\,\rho_{\Delta\lambda}}{\sum_{\Delta\lambda} E_{s\Delta\lambda}} \quad (5)$$

where $E_{s\Delta\lambda}$ is the incoming solar energy and $\rho_{\Delta\lambda}$ is the surface reflectance in wavelength interval, $\Delta\lambda$.

Precise estimation of BBA from NBR from a remote sensing image can be obtained when following three factors are accounted for: (i) the spectral reflectance characteristics of the surface of interest; (ii) the spectral distribution of the irradiance; and (iii) the wavelength region of the discrete spectral bands.

The AWiFS image has four narrow spectral bands in VIS (λ = 520-590 nm and 620-680 nm), NIR (770-860 nm) and SWIR (1550-1700 nm). The reflectance in these narrow bands (NBR) can be converted to the total BBA in the spectrum (400-2500 nm). Similarly, seven narrow spectral bands of MODIS image in VIS (459-479 nm, 545-565 nm and 620-670 nm), NIR (841-876 nm and 1230-1250 nm) and SWIR (1628-1652 nm and 2105-2155 nm) can be used for NBR to BBA conversion. To convert from NBR to BBA, however, an improved understanding of the relationship between the reflectance characteristics of the narrow bands with that of broad band for snow surfaces is required.

In the present paper, the spectrum was divided into different sub-regions: for AWiFS image the VIS sub region (400-700 nm); NIR sub region (700-1500nm) and SWIR sub region (1500-2500 nm). In case of MODIS image, different sub regions are VIS (400-500 nm, 500-600 nm and 600-700 nm), NIR (700-1000 nm and 1000-1500 nm), and SWIR (1500-2000 nm and 2000-2500 nm). The selection of the sub regions depends primarily on: (i) consistency of data in AWiFS and MODIS narrow spectral bands in these regions; (ii) independence in spectral reflectance characteristics of snow surface in these regions. It is very important here to examine the relationships between AWiFS and MODIS spectral bands and their corresponding sub region as mentioned above.

The total BBA for AWiFS image considering solar irradiance in the three sub-regions (i.e., VIS, NIR, and SWIR) can be represented as:

$$a_{AWiFS} = \frac{\sum_{\Delta\lambda 1} E_{s\Delta\lambda 1}\ \rho_{\Delta\lambda 1} + \sum_{\Delta\lambda 2} E_{s\Delta\lambda 2}\ \rho_{\Delta\lambda 2} + \sum_{\Delta\lambda 3} E_{s\Delta\lambda 3}\ \rho_{\Delta\lambda 3}}{\sum_{\Delta\lambda} E_{s\Delta\lambda}} \quad (6)$$

where the wavelength interval $\Delta\lambda$ represents spectral region (400-2500 nm); $\Delta\lambda 1$, $\Delta\lambda 2$ and $\Delta\lambda 3$ correspond to three sub regions of the spectrum i.e. $\Delta\lambda 1$: 400-700 nm; $\Delta\lambda 2$: 700-1500 nm and $\Delta\lambda 3$: 1500-2500 nm. E_s and ρ are solar irradiance and reflectance respectively in different bands.

Similar to (6), the BBA for MODIS can be represented as:

$$a_{MODIS} = \frac{\sum_{\Delta\lambda m 1}^{\Delta\lambda m 7} E_{s\Delta\lambda m}\ \rho_{\Delta\lambda m}}{\sum_{\Delta\lambda} E_{s\Delta\lambda}} \quad (7)$$

where $\Delta\lambda_{m1-m7}$(m suffix for MODIS) represents seven sub regions of solar spectrum in VIS, NIR and SWIR. $E_{s\Delta\lambda m}$ and $\rho_{\Delta\lambda m1-m7}$ are the solar irradiance and reflectance corresponding to broadband sub regions in different wavelength bands, $\Delta\lambda_{m1-m7}$ $(\Delta\lambda_{m1}, \Delta\lambda_{m2}, \ldots, \Delta\lambda_{m7})$ respectively.

The estimated values of broadband reflectance obtained from (6) and (7) may be different from the narrow band reflectances in corresponding AWiFS and MODIS spectral bands respectively. Therefore, an adjustment factor that defines the relation between broad band and narrow band reflectance may be derived [30]. The adjustment factor quantifies the ratio of the reflected radiations within the narrow spectral bands to the reflected radiations of the corresponding broad band in VIS, NIR and SWIR regions. Let f_1 to f_3 and f_{1m} to f_{7m} be the adjustment factors for AWiFS and MODIS images respectively. Equation (6) for AWiFS can then be rewritten as:

$$a = \frac{f_1^{-1} E_{s\Delta\lambda v}\rho_{\Delta\lambda v} + f_2^{-1} E_{s\Delta\lambda n}\rho_{\Delta\lambda n} + f_3^{-1} E_{s\Delta\lambda s}\rho_{\Delta\lambda s}}{\sum_{\Delta\lambda} E_{s\Delta\lambda}} \quad (8)$$

where subscripts v, n and s refer to narrow VIS, NIR and SWIR bands of AWiFS sensor respectively. By comparing (6) with (8), f_1, f_2 and f_3 can be estimated for AWiFS as:

$$f_1 = \frac{\rho_{\Delta v}\ E_{s\Delta\lambda v}}{\sum E_{s\Delta\lambda 1}\ \rho_{\Delta\lambda 1}} \quad (9a)$$

$$f_2 = \frac{\rho_{\Delta n}\ E_{s\Delta\lambda n}}{\sum E_{s\Delta\lambda 2}\ \rho_{\Delta\lambda 2}} \quad (9b)$$

$$f_3 = \frac{\rho_{\Delta s}\ E_{s\Delta\lambda s}}{\sum E_{s\Delta\lambda 3}\ \rho_{\Delta\lambda 3}} \quad (9c)$$

Similarly, the adjustment factors, f_{1m} , f_{2m}, $\cdots$, f_{7m}, may be estimated for MODIS as:

$$f_{1m} = \frac{\rho_{\Delta v1}\ E_{s\Delta\lambda v1}}{\sum E_{s\Delta\lambda m1}\ \rho_{\Delta\lambda m1}} \quad (10a)$$

$$f_{2m} = \frac{\rho_{\Delta n2}\ E_{s\Delta\lambda n2}}{\sum E_{s\Delta\lambda m2}\ \rho_{\Delta\lambda m2}} \quad (10b)$$

$$f_{3m} = \frac{\rho_{\Delta v3}\ E_{s\Delta\lambda v3}}{\sum E_{s\Delta\lambda m3}\ \rho_{\Delta\lambda m3}} \quad (10c)$$

$$f_{4m} = \frac{\rho_{\Delta v4}\ E_{s\Delta\lambda v4}}{\sum E_{s\Delta\lambda m4}\ \rho_{\Delta\lambda m4}} \quad (10d)$$

$$f_{5m} = \frac{\rho_{\Delta n5}\ E_{s\Delta\lambda n5}}{\sum E_{s\Delta\lambda m5}\ \rho_{\Delta\lambda m5}} \quad (10e)$$

$$f_{6m} = \frac{\rho_{\Delta s6}\ E_{s\Delta\lambda s6}}{\sum E_{s\Delta\lambda m6}\ \rho_{\Delta\lambda m6}} \quad (10f)$$

$$f_{7m} = \frac{\rho_{\Delta s7}\ E_{s\Delta\lambda s7}}{\sum E_{s\Delta\lambda m7}\ \rho_{\Delta\lambda m7}} \quad (10g)$$

where subscripts v, n and s refer to narrow VIS, NIR and SWIR bands of MODIS sensor. $\Delta\lambda_{m1}$, $\Delta\lambda_{m2}$ ….., $\Delta\lambda_{m7}$ represent broadband sub-regions consistent with MODIS spectral bands.

Assuming a linear relationship between the narrowband and the broadband albedo [2, 9], the surface albedo from data of AWiFS and MODIS sensors can be estimated from:

$$a_{AWiFS} = C_1\,\rho_2 + C_2\rho_4 + C_3\rho_5 + d \quad (11)$$

$$a_{MODIS} = C_{1m}\,\rho_{1m} + C_{2m}\,\rho_{2m} + C_{3m}\,\rho_{3m} + C_{4m}\,\rho_{4m} + C_{5m}\,\rho_{5m} + C_{6m}\,\rho_{6m} + C_{7m}\,\rho_{7m} + d_m \quad (12)$$

where c's are coefficients, ρ's are narrow band reflectance in AWiFS and MODIS bands, and d is an offset, which is typically determined by comparing estimated values of albedo from model with those obtained from in-situ observations. On combining (8), (9) and (11), the values of coefficients may be estimated as:

$$c = wf^{-1} \quad (13)$$

where w's are the percentages of solar radiation within the wavelength bands of AWiFS and MODIS channels considered respectively. This is estimated using in-situ observations of solar spectral irradiance (Fig. 6). The values of f are calculated using the in-situ observations of spectral reflectance and spectral irradiance in (9) and (10) recorded at the time of satellite pass.

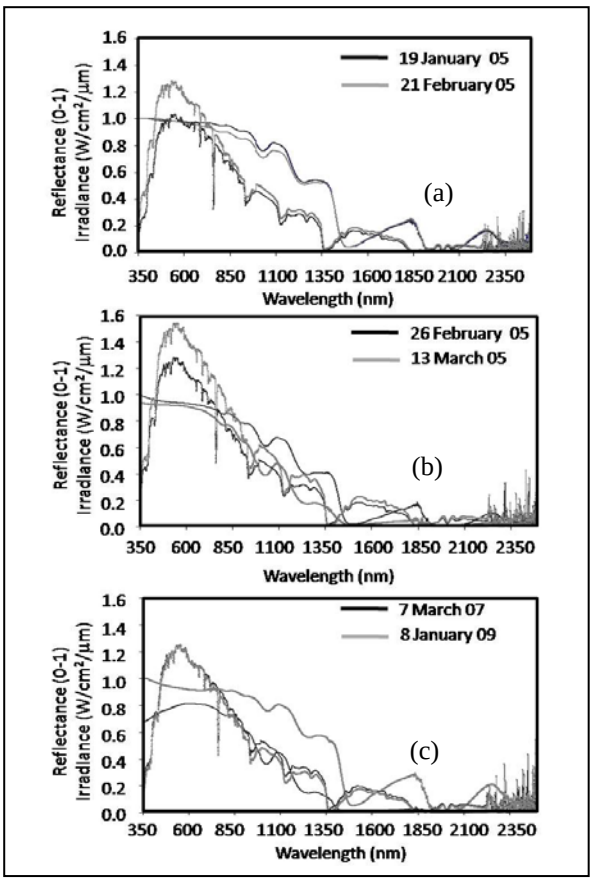

Fig. 6 Field observations of spectral reflectance (0-1) and transmitted solar spectral irradiance for different dates of AWiFS acquisition

VII. RESULTS AND DISCUSSION

A. Spectral Reflectance and Spectral Irradiance

The upwelling 't_v' and downwelling 't_z' transmissivity due to Rayleigh scattering from ground to sensor and sun to ground respectively for AWiFS and MODIS bands are given in the Table IV. Fig. 6 shows the average spectral reflectance characteristics of snow surface and spectral distribution of transmitted solar irradiance at different sampling locations surrounding Solang and Dhundi during six different passes of satellite carrying AWiFS sensor. It can be inferred from these figures that snow is characterized by high spectral reflectance in the visible part of an electromagnetic spectrum. It tends to decline in the near infrared region until 1050 nm wavelength, where marginal increase in reflectance occurs. A minor peak in reflectance can be seen at approximately 1090 to 1100 nm wavelength. The minor peaks can also be seen at around 1800nm and 2250nm wavelength with a sharp dip in reflectance at about 1950 nm to 2050nm. This is due to the presence of water absorption bands at these wavelengths. The transmitted solar irradiance (Figs. 6a-c) has been found to be the maximum in visible wavelength region with a gradual decrease with increase in wavelength. The irradiance contribute 46.2 % in 400-700 nm, 26.8% between 700-1000 nm, 16.7% in 1000-1500 nm and 10.2% in 1500-2500 nm wavelength regions.

These in situ observations have also been used to:

i) establish a relationship between existing narrow AWiFS and MODIS wave bands and corresponding broadband for estimation of values of the conversion factor f using (9) and (10);

ii) estimate BBA and its validation with AWiFS satellite sensor albedo.

The values of empirical coefficient, C, for AWiFS and MODIS sensors have been estimated using (13) and are given in the Table V.

TABLE V MODEL COEFFICIENTS FOR AWIFS AND MODIS TO CONVERT NARROW BAND TO BROAD BAND ALBEDO

AWiFS Coefficient		MODIS Coefficient	
C_1	0.463	C_{1m}	0.145
C_2	0.360	C_{2m}	0.275
C_3	0.094	C_{3m}	0.138
d	0.026	C_{4m}	0.165
-	-	C_{5m}	0.214
-	-	C_{6m}	0.06
-	-	C_{7m}	0.06
-	-	d_m	-0.011

B. Broadband Albedo (BBA) and Validation

In this section, results of satellite sensor estimated snow BBA and their validation with in-situ observations at Solang, Dhundi and Patsio sites have been presented. The non-snow area in satellite images is masked using normalized difference snow index (NDSI >= 0.4) and reflectance in NIR > 0.10 [31]. Broadband albedo validation details at different sites are given below:

1) Validation at Solang and Dhundi Sites Using Awifs Image:

Figs. 7 (a-f, g-l) show the topographically uncorrected and corrected AWiFS reflectance images of Beas basin respectively. The thematic maps of (surrounding Solang and Dhundi) radiometrically corrected BBA obtained using (11) for snow covered regions are shown in the Figs. 7 (m-r). The value of radiometrically corrected broadband albedo of snow in these maps varies from 0.2 to 0.9.

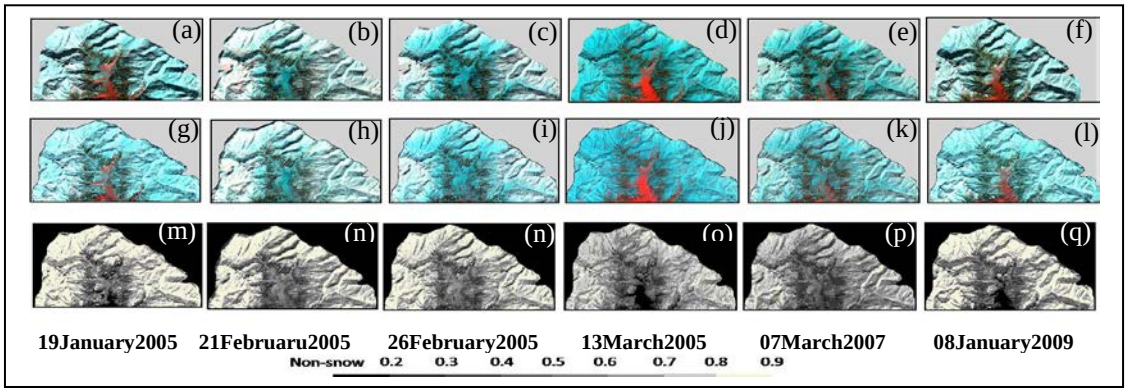

Fig. 7 (a-f) Topographically uncorrected AWiFS images of different dates of Beas Basin (surrounding Solang and Dhundi); (g-l) Topographically corrected images; and (m-r) Thematic maps of broadband albedo for snow covered region after masking non-snow area

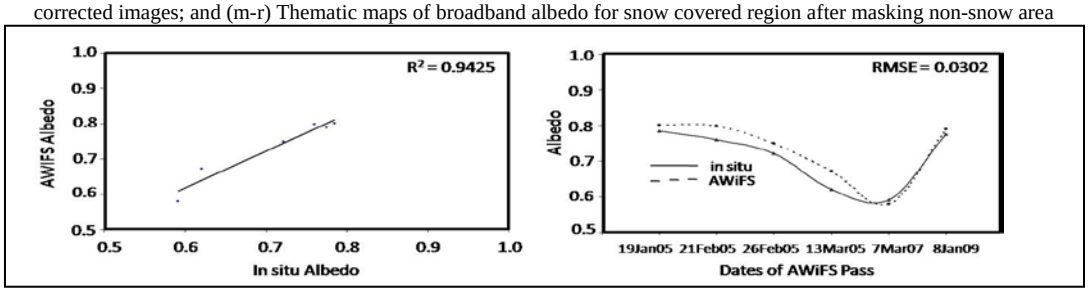

Fig. 8 Comparison of the retrieved snow broadband albedo with the in-situ measurements at sites Solang and Dhundi

In majority of the area, higher values (0.7-0.9) can be seen for the data acquired during January and February months than those obtained for the month of March, where the albedo in most of the snow area ranges from 0.5-0.7. This decrease may be attributed to the melting of snow during this month. The results on validation of satellite estimated BBA of snow using AWiFS with in-situ observations (data obtained using optical spectroradiometer) are shown in the Fig. 8. The overall R^2 between observed and estimated values exceeds 0.94. The corresponding RMSE value has been determined as 0.03. These values indicate that the estimated BBA retrievals for AWiFS image bear a close relationship but may not be considered as identical to the in situ measurements (Fig. 8). This may be attributed to the mismatch in spatial resolution of the image 56 m with in situ measurements, which happen to be point data.

2) Validation at Patsio Sites Using Awifs and MODIS Data:

The Patsio site lies in the middle Himalaya where the temperatures are quite low as discussed earlier. The snow BBA measured from albedometer on AWS has been used for validation of BBA estimated from proposed algorithm applied at Patsio site. Topographically uncorrected and corrected AWiFS reflectance images of lower and middle Himalaya (all three stations Solang, Dhundi and Patsio sites) have been shown in the Figs. 9 (a-g, h-n) respectively. Figs. 9(o-u) show the thematic maps of snow BBA, which have been validated with in-situ albedo measurements at Patsio site. Fig. 10 shows the relationships between (AWiFS) retrieved snow broadband albedo with the in-situ measurements at Patsio site. The overall R^2 between measured and estimated values for AWiFS data exceeds 0.94 and the RMSE has been obtained as 0.0274. The R^2 value and RMSE show that the AWiFS estimated BBA is in close agreement with the in-situ measurements at the Patsio site.

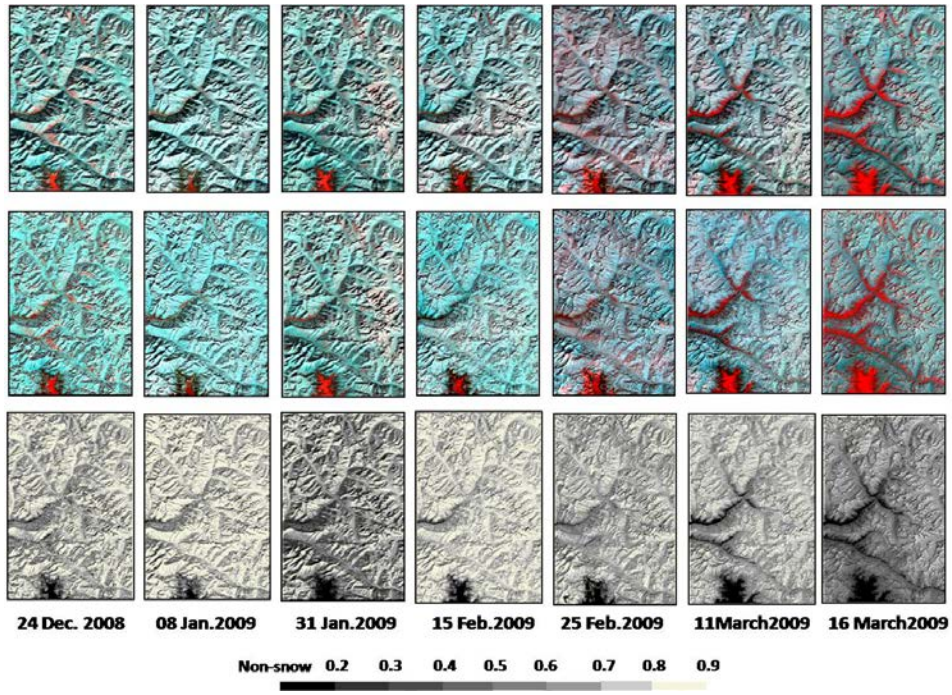

Fig. 9 (Top Row) Uncorrected AWiFS images of different dates includes all three sites Solang, Dhundi and Patsio; (Middle Row) Atmospherically and topographically corrected images; and (Bottom Row) Thematic maps of broadband snow albedo after masking non snow area

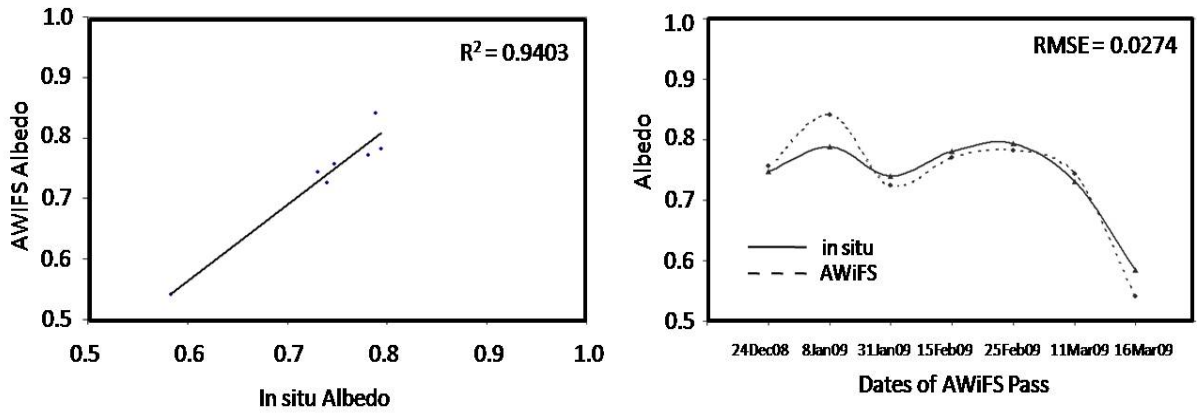

Fig. 10 Comparison of the satellite (AWiFS) retrieved snow broadband albedo with the in-situ measurements at site Patsio

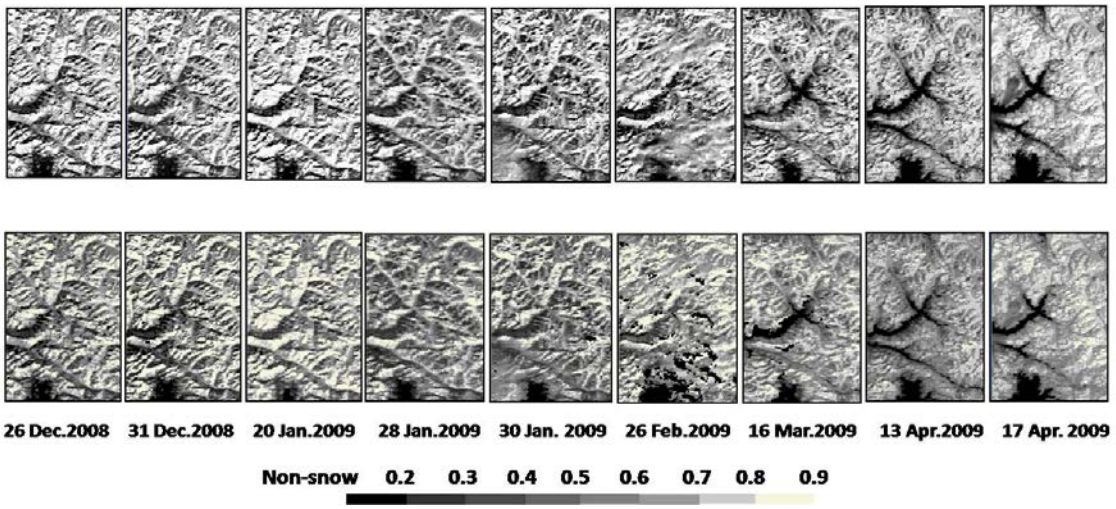

Fig.11 (First Row) MODIS images of different dates includes all three sites Solang, Dhundi and Patsio; (Second Row) Thematic maps of broadband snow albedo after masking non snow area

The snow BBA estimated from MODIS images at Patsio site has been validated with in-situ observations and global albedo model proposed by [11]. Figs. 11 (a-i) show the atmospherically corrected MODIS images of different dates. Corresponding thematic maps of BBA for snow covered region are shown in the Figs. 11 (j-r). Fig. 12 (a) shows the correlation between MODIS estimated BBA of snow using proposed model and in-situ observed albedo at Patsio site while Fig. 12 (b) shows the correlation between MODIS estimated BBA of snow using [11] model and in-situ observed albedo at the same site. Fig. 12 (c) shows the RMSE of the proposed model and Liang model [11]. A high correlation (R^2 = 0.88 for proposed model, and R^2 = 0.84 for Liang model) and low RMSE (0.026 for proposed model and 0.031 for Liang model) have been observed between estimated albedo and in-situ measured albedo for both the models although proposed model performed slightly better for the validation site.

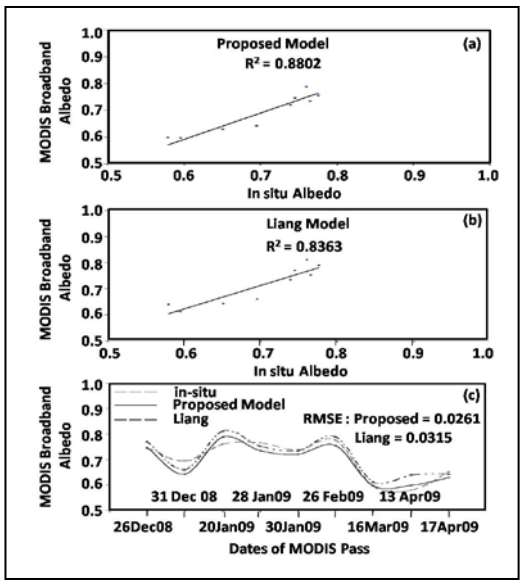

Fig. 12 Validation of the satellite (MODIS) retrieved snow broadband albedo with the in situ measurements at site Patsio (a) Proposed Model (b) Liang Model (c) RMSE

The performance of the proposed model has also been tested rigorously for a large snow covered region of Himalaya shown in Figs. 13 (a-b) vis-a-vis global albedo model proposed by [11] for nine images of different dates. A high value of correlation (R^2 better than 0.99) and a low value of RMSD (0.015) have been observed between the two models (Fig. 14) for snow covered region. The global albedo model developed by [11] has not been validated for snow and ice, although the model is validated for other land covers. These results show that the Liang model is also performing well for snow and ice land covers.

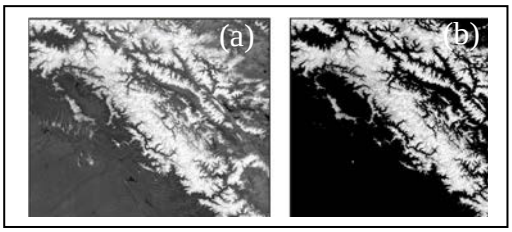

Fig. 13 (a) MODIS image of large snow covered Himalayan region and (b) Snow covered region after masking non snow area used for comparative analysis between proposed broadband snow albedo model and Liang global model

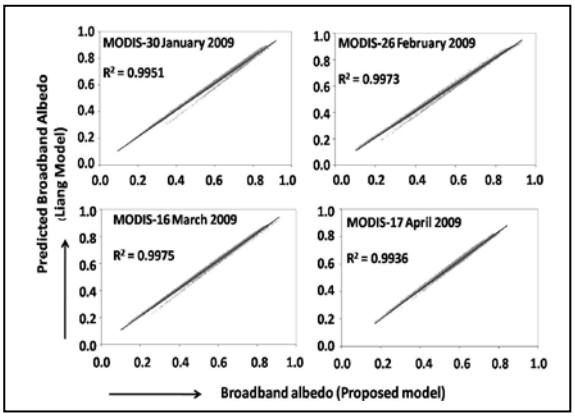

Fig. 14 Comparative and correlation analysis between proposed snow broadband albedo and Liang global model using different dates MODIS data

VIII. CONCLUSIONS

Snow surface broadband albedo is a fundamental component in modeling any surface processes. In this paper, an operational algorithm for direct retrieval of snow broadband albedo using AWiFS and MODIS data has been developed and presented. This appears to be the first algorithm reported to estimate braodband albedo of snow from narrow band reflectances using AWiFs images in the Himalayan region. The in-situ measurements of spectral reflectance and transmitted solar irradiance have been used for estimation of conversion factor and coefficients required for development of snow broadband albedo using AWiFS and MODIS data. The results of BBA of snow retrieved from AWiFS and MODIS have also been validated with in-situ measurements at Solang, Dhundi and Patsio sites. The overall R^2 and RMSE values between in-situ observed and estimated BBA for AWiFS were observed better than 0.94 and 0.03, while for MODIS data it were 0.88 and 0.026 respectively. For MODIS data, the results from the proposed algorithm have also been found to be in agreement (overall R^2, 0.99 and RMSD, 0.015) with published global albedo model for the large Himalayan snow cover region.

ACKNOWLEDGEMENTS

We would like to thank Shri Ashwagosha Ganju, Director of Snow & Avalanche Study Establishment (SASE) for constant motivation for the study. We also thank Dr. P.K. Satyawali, internal reviewer of the manuscript for his valuable suggestions.

REFERENCES

[1] A. G. Klein and J. Stroeve, “Development and validations of a snow albedo algorithm for the MODIS instrument,” Annals of Glaciology, vol. 34, pp. 45-52, 2002.

[2] J. Stroeve and A. Nolin, “New methods to infer snow albedo from the MISR instrument with applications to the Greenland ice sheet,” IEEE Transaction of Geoscience & Remote Sensing, vol. 40, No.7, pp. 1616 – 1625, 2002a.

[3] C.R. Duguay and E. F. Ledrew, “Mapping surface albedo in the East slope of the Colorado front range, U.S.A., with LANDSAT THEMATIC MAPPER,” Arctic and Alpines Research, vol. 23, No.2, pp. 213 -223, 1991.

[4] H. S. Gusain, A. Singh, A. Ganju and D. Singh, “Characteristics of the seasonal snow cover of Pir Panjal and Great Himalayan ranges in Indian Himalaya,” International symposium on snow monitoring and avalanches, 12-16 April, Manali, India, 2004.

[5] H.S. Negi, A.V. Kulkarni and B.S. Semwal, “Estimation of snow cover distribution in Beas Basin, Indian Himalaya using satellite data and ground measurements,” Journal of Earth System Science, vol. 118, No. 5, pp. 525-538, 2009.

[6] S. Liang, C. J. Shuey, A. L. Russ, H. Fang, M. Chen, C. L. Walthall, C. S. T. Daughtry and R. Hunt, Jr., “Narrowband to broadband conversions of land surface albedo : II validation,” Remote Sensing of Environment, vol. 84, pp. 25-41, 2002.

[7] J. Key, X. Wang, J. Stroeve and C. Fowler, “Estimating the cloudy sky albedo of sea ice and snow from space,” Journal of Geophysical Research, vol. 106, No. D12, pp. 12,489-12,497, 2001.

[8] J. Stroeve, “Assessment of Greenland albedo variability from the advanced very high resolution radiometer Polar Pathfinder data set,” Journal of Geophysical Research, vol. 106 , pp. 33,989 - 34,006, 2001.

[9] J. Stroeve, A. Nolin. “Comparison of MODIS and MISR derived surface albedo with in situ measurements in Greenland,” EARSeL ePROC, vol. 2, No. 1, pp. 88-96, 2002b.

[10] S. Liang, A. Strahler, C. Walthall. “Retrieval of land surface albedo from satellite observations: A simulation study,” Journal of Applied Meteorology, vol. 38, pp. 712-725, 1999.

[11] S. Liang, “Narrowband to broadband conversions of land surface albedo I Algorithms,” Remote Sensing of Environment, vol. 76, pp. 213-238, 2000.

[12] S. Liang, “A Direct algorithm for estimating land surface broadband albedo from MODIS imagery,” IEEE Transaction of Geoscience & Remote Sensing, vol. 41, No. 1, pp. 136-145, 2003.

[13] S. S. Sharma and A. Ganju, “Complexities of avalanche forecasting in Western Himalaya - An Overview,” Cold Regions Science and Technology, vol. 31, pp. 95-10, 2000.

[14] PS Jr., Chavez, “Radiometric calibration of Landsat Thematic Mapper multispectral images,” Photogrametric Engineering and Remote Sensing, vol. 55, pp. 1285 – 1294, 1989.

[15] C. Song, C.E. Woodcock, K.C. Seto, M.P. Lenney and A.S. Macomber, “Classification and change detection using Landsat TM data: when and how to correct atmospheric effects,” Remote Sensing of Environment, vol. 75, pp. 230 – 244, 2001.

[16] V. D. Mishra, J. K. Sharma, K.K. Singh, N. K. Thakur, and M. Kumar, “Assessment of different topographic corrections in AWiFS satellite imagery of Himalaya terrain,” Journal of Earth System Science, vol. 118, No. 1, pp. 11-26, 2009.

[17] Y. Liu, Y. Noumi, Y. Yamaguchi, “Discrepancy between ASTER- and MODIS- derived land surface temperature: Terrain Effects,” Sensors, vol. 9, pp. 1054-1066, 2009.

[18] Y. Kim and K. Lee, “An experimental study on the Image - Based atmospheric correction method for high resolution multispectral data,” IEEE Transaction of Geoscience Remote Sensing, pp. 434-436, 2005.

[19] V. D. Mishra, H. S. Negi, A. K. Rawat, A. Chaturvedi, R.P. Singh, “Retrieval of sub-pixel snow cover information in the Himalayan region using medium and coarse resolution remote sensing data,” International. Journal of Remote Sensing, vol. 30, No. 18, pp. 4707 – 4731, 2009.

[20] P. B. Russell, J. M. Livingston, E.G. Dutton, R. F. Pueschel, J. A. Reagan, T. E. Defoor, M. A. Box, D. Allen, P. Pilewskie, B. M. Herman, S. A. Kinne and D. J. Hoffman, “Pinatubo and Pre-Pinatubo optical depth spectra: Mauna Loa measurements, compositions, inferred particle distribution, radiative effects, and relationship to lidar data,” Journal of Geophysical Research, vol. 98, pp. 22969–22985, 1993.

[21] PS Jr., Chavez, “An improved dark object subtraction technique for atmospheric scattering correction of multispectral data,” Remote Sensing of Environment, vol. 24, pp. 459–479, 1988.

[22] PS Jr., Chavez, Image based atmospheric corrections revisited and improved. Photogrammetric Engineering and Remote Sensing, vol. 62, pp. 1025 – 1036, 1996.

[23] M.S. Moran, R.D. Jackson, P.N. Slater and P.M. Teillet, “Evaluation of simplified procedures for retrieval of land surface reflectance factors from satellite sensor output,” Remote Sensing of Environment, vol. 41, pp. 169–184, 1992.

[24] M. R. Pandya, R. P. Singh, K. R., Babu, P.N. Murali, A. S. Kirankumar and V. K. Dadhwal, "Bandpass solar exo-atmospheric irradiance and Rayleigh optical thickness of sensors on board Indian Remote Sensing satellites - 1B, 1C, 1D and P4," IEEE Transaction of Geoscience Remote Sensing, vol. 40, No. 3, pp. 714-717, 2002.

[25] F. Kasten "Table of solar altitudes for geographical latitudes," CRREL Special Report 57 U.S. Army Corps of Engineers, Hanover, New Hampshire, 1962.

[26] F. Van Der Meer, "Spectral mixture modeling and spectral stratigraphy in carbonate lithofacies mapping," ISPRS Journal Photogrammetric and Remote Sensing, vol. 51, pp. 150 – 162, 1996.

[27] D. L. Civco, "Topographic normalization of Landsat Thematic Mapper digital imagery," Photogrammetric Engineering and Remote Sensing, vol. 55, pp. 1303-1309, 1989.

[28] J. D. Colby, "Topographic normalization in rugged terrain," Photogrammetric Engineering and Remote Sensing, vol. 55, pp. 531-537, 1991.

[29] J. Nichol, L. K. Hang and W. M. Sing, "Empirical correction of low sun angle images in steeply sloping terrain: a slope matching technique," International Journal of Remote Sensing, vol. 2, No. (3-4), pp. 629-635,2006.

[30] J. Song and W. Gao, "An improved method to derive surface albedo from narrowband AVHRR satellite data: Narrowband to broadband conversion," Journal of Applied Meteorology, vol. 38, pp. 239-249, 1999.

[31] M. Singh, V. D. Mishra, N. K. Thakur, A. V. Kulkarni and M. Singh, "Impact of climatic parameters on statistical stream flow sensitivity analysis for hydro power," Journal of Indian Society Remote Sensing, vol. 37, pp. 573-586, 2009.

Varunendra Dutta Mishra received the M.Sc. degree in Physics and Ph.D. in condensed matter physics from Indian Institute of Technology, Delhi, India in 1989 and 1996 respectively. He was appointed as a scientist in April 1996 in Snow & Avalanche Study Establishment (SASE) and continuing till now in Chandigarh, India. He has worked in various projects on remote sensing sanctioned by Government of India. His primary research interest is topography and modeling snow physical parameters using optical and passive microwave remote sensing in North West Himalaya. He received various awards like Technology Group Award, Science Day Award, and Best scientific paper award by SASE and Indian Society of Remote Sensing, India. He has published 26 papers in refereed National, International journal and contributed 18 in National and International conferences. He is a life member of Indian Society of Remote Sensing.

Hemendra Singh Gusain received his M.Sc. degree in Physics in 1996 from H.N.B Garhwal University, Srinagar, Garhwal and M.Tech degree in 2001 in Cold Region Science and Engineering from G.B.Pant university of Agriculture and Technology, Pantnagar, India. He is pursuing his Ph.D. from Indian Institute of Technology, Roorkee, India. His present research interest is geo-spatial modeling of snow physical properties and climatic variability using remote sensing and in-situ observations.

Prof. Manoj Arora received his B.E. in Civil Engineering from Punjab Engineering College, Chandigarh and M.E. degree in Survey and photogrammetry from I.I.T. Roorkee (Formerly University of Roorkee) in 1984 and 1986 respectively. He completed his Ph.D. in 1996 from university of Wales Swansea (UK) in remote Sensing. Presently he is working as a professor in Geomatics, Department of Civil Engineering IIT Roorkee. His research interest is land cover mapping, digital image classification, neural network and fuzzy logic, remote sensing, GIS and GPS applications, SAR interferometry, land slide hazard. He has supervised more than 15 Ph.D. scholars. He has published more than 75 papers in national and international journal of repute. He received prestigious young teacher career award by AICTE and outstanding professor from IIT Roorkee.